Experimental and Theoretical Reinvestigation of CO Adsorption on Amorphous Ice

C. Manca, C. Martin, A. Allouche, and P. Roubin*

Physique des Interactions Ioniques et Moléculaires UMR 6633, Université de Provence, Centre Saint Jérôme (case 242), 13397 Marseille Cedex 20, France

Received: August 8, 2001; In Final Form: September 27, 2001

We have performed new quantum calculations based on density functional theory, using plane waves and ultrasoft pseudopotentials to deal with the problem of modeling CO adsorption on a water ice surface and to obtain a theoretical understanding on the physical mechanisms involved during the monolayer formation. We have also done a new series of experiments, using the combination of volumetric adsorption isotherm and infrared spectroscopy measurements to study the different stages of CO adsorption on amorphous ice, from submonolayer to solid condensation. The multilayer formation has been evidenced by volumetric measurements, and its contribution has been characterized in the low-frequency part of the CO infrared spectrum. Three surface sites have been identified by spectroscopy, and their intensities have been controlled throughout the whole monolayer formation, showing a site specific, though nonselective, adsorption process. Calculations have consistently succeeded in determining three adsorption configurations whose energies are similar. Finally, the geometry of the complete monolayer has been fully described, and its high compacity has been explained by analyzing the balance between vertical and lateral interactions.

I. Introduction

The study of the interaction of atoms and molecules with water ice surfaces has focused interest for several years because of its importance for atmospheric chemistry (Arctic and Antarctic polar ices,[1,2] stratospheric clouds,[3,4] and the Antarctic ozone hole[5]) and also for astrochemistry (icy mantle of interstellar grains,[6] planetary ices, and ices in comet tails[7−9]). Infrared spectroscopy has proved to be a powerful tool of investigation and a typical example has been given by the recent results of the short wavelength spectrometer (SWS) on board the IR space observatory (ISO).[10]

In condensed state, each H_2O molecule can form four hydrogen bonds (two as proton donor and two as proton acceptor) with four other H_2O molecules in a tetrahedral arrangement: if the surface is a simple breaking of the bulk symmetry, three sorts of surface molecules are expected and have actually been characterized, two of three-coordinated molecules and one of four-coordinated molecules. Three-coordinated molecules with an OH group noninvolved in a hydrogen bond will be referred to as a dangling H (dH) molecule, using Devlin's notation.[11] In the same way, three-coordinated molecules with an oxygen electronic pair noninvolved in a hydrogen bond will be referred to as a dangling O (dO) and a four-coordinated molecule with their distorted tetrahedron, as s4. Figure 1 displays a schematic top view of the water molecules at the surface showing the arrangement of dH, dO, and s4 (s4a and s4b) molecules.

The infrared signal of ice in the OH stretching mode domain is composed of a very broad band centered at 3250 cm^{-1} due to the in-bulk molecules and a weak band at 3696 cm^{-1} due to the dH molecules.[12] Another band at 3720 cm^{-1}, only observed in the case of ice deposited at very low temperatures, has been assigned to two-coordinated molecules[13] and will not be considered here. The dH band strongly depends on the interaction of dH with molecules and is always shifted toward lower frequencies by adsorption.

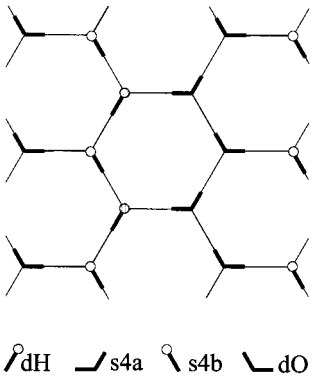

Figure 1. Schematic of the top view of ice surface.[51] OH bonds roughly in the surface plane (respectively above and below) are indicated in bold line (respectively solid circle and open circle).

The CO/amorphous ice system has been the subject of many experimental studies.[14−19] The main reasons are (i) CO is one of the major components of the interstellar medium; (ii) CO possesses a small dipole moment and its affinity for water is poor; thus, it may not strongly disturbed the ice surface; and (iii) the vibrational spectrum of CO has already proved to be a good probe for various other solid surfaces (metals,[20] metal oxides, ionic solids,[21−25] zeolites,[26−30] etc.).

The spectral response of CO adsorbed on amorphous ice is a doublet (which we have measured at 2154 and 2139 cm^{-1}),[31] and different assignments have already been attempted.[14,16,19] In a previous work performed in our laboratory[19] (referred to as paper I in what follows), isotherms deduced from the infrared signal of CO have been measured, with the sample being maintained under vacuum, and results have then been compared to Periodic Hartree−Fock quantum calculations (PHF). In the present work, a new experimental setup allows us to perform

* To whom correspondence should be addressed. E-mail: proubin@piima1.univ-mrs.fr.

10.1021/jp013100f CCC: $20.00
Published on Web 11/30/2001

volumetric isotherms and infrared spectroscopy simultaneously, with the sample being in equilibrium with the gas phase. We can thus control the adsorbed amount and study modifications in the infrared spectrum of both ice and adsorbate at different stages of adsorption.[31,32] This combination of experimental techniques is well suited to fully elucidate the origin of the CO multiplet. Few theoretical studies,[19,33,34] and among them quantum studies (paper I), have tried to explain the interactions between water and CO. We have developed here new calculations based on density functional theory using plane wave basis set and ultrasoft pseudopotentials (DFT-PW). This allows us to deal with large periodic systems and to model the adsorption of several CO molecules per ice cell.

Therefore, we have decided to revisit CO adsorption on amorphous ice using these improved experimental and theoretical methods, the aim being to compare the two sets of results and to deduce information about the structure and the dynamics of adsorption. This paper is organized in three sections: the experimental method is explained in section II, and the information provided is compared to that of paper I. The improvement in calculations, from PHF to DFT-PW, is described in section III, and a model for the progressive coverage of the ice surface is proposed. A comparison of experimental and theoretical results is achieved in the general discussion of section IV.

II. Experimental Section

A. Experimental Setup and Ice Sample Preparation. Volumetric isotherms and infrared measurements were performed simultaneously, with the sample being in a copper cell with two sapphire windows enabling infrared spectra to be collected in the range of 4000−1600 cm^{-1} in the transmission mode. The cell was connected to a stainless steel volume and was enclosed in a cryostat with KBr windows, continuously maintained under a vacuum lower than 10^{-4} Pa and cooled by a CTI CRYOGENICS model 22 closed-cycle helium cryocooler. It was possible to regulate the cell temperature between 20 and 300 K using a Lake Shore Cryotonic, Inc., controller connected to a diode (model DT500) fixed on the cell. The equilibrium pressure was measured in a range of 10^{-1}−10^{5} Pa using two DATAMETRICS Barocel type 570 pressure sensors (in the ranges of 0−10 Torr and 0−1000 Torr). Infrared spectra were collected using a Nicolet 7199 FTIR spectrometer. The resolution was 1 cm^{-1}, and 200 scans were collected per spectra.

Ice samples were prepared as follows: a gas mixture H_2O:Ar (1:30) was rapidly sprayed (roughly 0.3 $mol.h^{-1}$) into the cell maintained at 40 K under vacuum, with argon being trapped together with water. Then, the sample was pumped and slowly annealed (0.2 K min^{-1}) for 5 h to 90 K, thus permitting argon to desorb and amorphous ice to be formed. Finally, the ice sample (approximately 2−3 mg) was cooled at the temperature chosen for the isotherm. Its specific surface area, measured using CH_4 as probe molecule,[31] was higher than 100 $m^2\ g^{-1}$. Figure 2 shows a typical infrared spectrum of our samples. The broad band between 3600 and 3000 cm^{-1} centered at roughly 3250 cm^{-1} is mainly assigned to the bulk modes of ice, whereas the weak peak at 3696 cm^{-1} is assigned to the well-known dH mode.[13] The whole spectrum is analogous to those previously published for amorphous ice.[19,35] The chemical purity of carbon monoxide (Alpha Gaz) was 99.997%. The temperatures mentioned in this paper were determined by measuring the saturation pressure of CO and by using Clapeyron's law.

Point by point isotherms were performed and for each step, the value of equilibrium pressure p was measured, and the infrared spectrum was recorded. We were thus able to quantify the adsorbed amount and to measure alterations in the vibrational modes of both the ice surface and the adsorbate, from submonolayer to bulk. At the end of the experiment (i.e., when saturation pressure p^0 was reached), the adsorbate was desorbed. We then checked that the ice surface had not been disturbed during a cycle of adsorption−desorption by comparing infrared spectra of bare ice before and after each cycle.

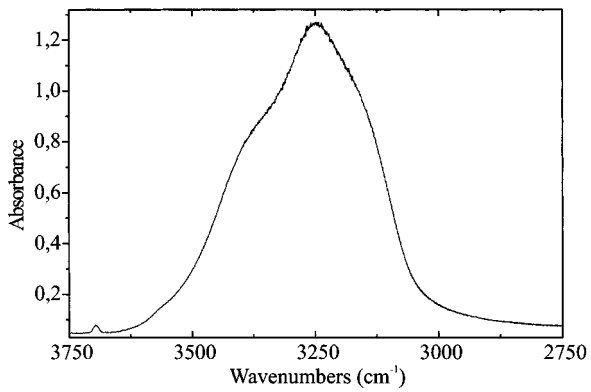

Figure 2. Infrared spectrum of a sample of amorphous ice obtained by a mixture H_2O:Ar (1:30) deposited at 40 K, annealed at 90 K, and recooled at 40 K. The dangling H mode is reported at 3696 cm^{-1}.

B. Methods. According to the Brunnauer, Emmet, and Teller (BET) model,[36] adsorption occurs by the formation of stacks of molecules on each surface adsorption site. The adsorption of a molecule on a vacant (respectively already occupied) site is characterized by energy ϵ (respectively ϵ'), and the difference between these two energies is the net heat of adsorption ΔQ. This model has already been used in paper I with isotherms deduced from the CO infrared signals, using the ratio A/A_0 directly related to the surface coverage θ (A was the integrated absorbance of the CO bands, and A_0 was that at monolayer completion). With the new setup, we were able to measure equilibrium pressure p and to control the adsorbed amount of molecules. We decided to use the common form of the BET equation:

$$v_{ads} = \frac{v_m C\, p/p^0}{(1 - p/p^0)(1 + (C-1)p/p^0)} \qquad (1)$$

with v_{ads} being the volume of the molecules adsorbed on the surface, v_m being the monolayer capacity, and C being the BET constant from which ΔQ is estimated:

$$C \simeq \exp\left(\frac{\Delta Q}{RT}\right) \qquad (2)$$

Whenever adsorption occurs rather than condensation, positive values of ΔQ are found. According to previous results obtained on different materials,[37] the fit of the linear form of eq 1 must be performed in a limited range of relative pressure ($0.05 < p/p^0 < 0.35$). BET values were calculated here using experimental points within this range, allowing us to estimate ΔQ and v_m.

We used here the isosteric method to estimate the isosteric heat of adsorption q^{st}. Assuming that q^{st} does not vary with temperature, an equation analogous to that of Clausius−Clapeyron for a given surface coverage θ is found:

$$\left(\frac{\partial[\ln p])}{\partial(1/T)}\right)_\theta = -\frac{q^{st}}{R} \qquad (3)$$

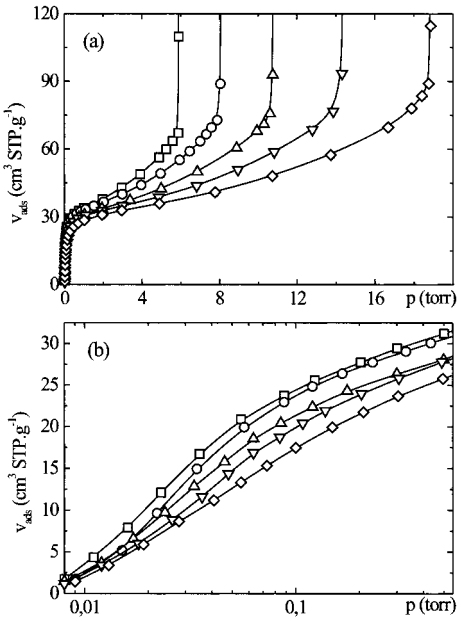

Figure 3. (a) Volumetric isotherms of CO on amorphous ice at different temperatures: (□) 56.3, (○) 57.3, (△) 58.3, (▽) 59.3, (◇) and 60.3 K. (b) The same isotherms in the region of the monolayer completion, with the axis of the relative pressure being in logarithmic scale. Continuous lines are only a guide for the eyes.

The isosteric method of calculating q^{st} consists of performing a series of adsorption isotherms in a short range of temperature and of plotting [ln p] as a function of $1/T$ to determine the slope of the curve. A major interest of this method is that it gives q^{st} for various surface coverages and not only for $\theta = {}^1/_2$ as in paper I, with the aim being here to estimate the interaction between adsorbate and substrate as well as lateral interactions between adsorbed molecules.

The correlation between the two measurements (adsorption isotherm volumetry and infrared spectroscopy) has been described in detail in a previous paper.[31] Various isotherms, which we will call *infrared* isotherms, have been obtained by plotting the evolution of the integrated absorbance of various infrared bands of ice or of adsorbed CO as a function of relative pressure. In the case of CO, we obtained the infrared signal of both the adsorbed phase and the gas phase. We eliminated the signal of the gas phase by subtracting the signal recorded for CO at the same temperature, without the ice sample, and we measured the integrated absorbance of the selected signals for each value of the relative pressure. Finally, the curves were arbitrarily normalized, if necessary to display the whole set of results in a single figure. We were thus able to make a comparative analysis of the information given by both kinds of isotherms (*volumetric* and *infrared*). It is worth noting that we were sure that no solid CO was formed before $p = p^0$ because we were continuously at thermodynamic equilibrium, and this allowed the multilayer formation to be studied.

C. Results. Figure 3a shows a series of adsorption isotherms of CO on amorphous ice within the range of 56−60 K. In Figure 3b, these isotherms are plotted in a logarithmic scale to focus on the monolayer completion. They are type II isotherms: v_{ads} first rises abruptly during the monolayer formation, and then, the rate of the growth clearly decreases during the multilayer formation, with the transition between these two regimes, i.e., the knee of the isotherm, occurring at the monolayer completion. Finally, it rises again abruptly at $p = p^0$ during the bulk condensation.

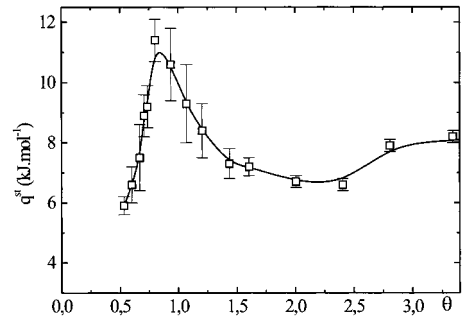

Figure 4. Isosteric heat of adsorption q^{st} of CO on amorphous ice for $56.3 < T < 60.3$ K as a function of the surface coverage θ. Each point corresponds to the value of the slope of [ln $p = f(1/T)$] using the isosteric method, with the error bars showing the linear fit error and the continuous line being a guide for the eyes.

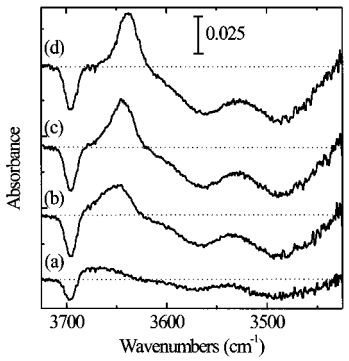

Figure 5. Infrared difference spectra (CO adsorbed on ice at $T = 56.3$ K minus bare ice) in the region of the surface-localized modes of ice for surface coverage θ (a) 0.21, (b) 0.73, (c) 0.92, and (d) 3.80.

We used the BET theory to evaluate v_m, C, and ΔQ. We found the same value of monolayer completion ($v_m = 27$ cm^3 STP g^{-1}) for the five isotherms showing both that the different BET fits are consistent and that the sample had not been disturbed during the adsorption−desorption cycle. We found ΔQ at 2.9 ± 0.3 kJ mol^{-1}, close to previous results,[19,38] and this low value reflects the weak interaction between ice and carbon monoxide. ΔQ is approximately the difference, at the monolayer completion, between isosteric heat of adsorption q^{st} and heat of condensation[39] which is 8.3 kJ mol^{-1}. By this way, we estimate q^{st} at 11.3 ± 0.3 kJ mol^{-1}, and this value will now be compared with that determined by the isosteric method.

Figure 4 shows the evolution of q^{st} as a function of surface coverage θ which is the ratio between v_{ads} and v_m. No values of q^{st} are given for $\theta < 0.5$ because the error on the equilibrium pressure at low surface coverage is too important to obtain reliable results. For $0.5 < \theta < 1$, q^{st} increases, whereas for $\theta > 1$, q^{st} decreases to a value close to the heat of condensation. The highest value (11.4 kJ mol^{-1}), obtained near the monolayer completion, is in good agreement with that previously obtained by the BET fit. q^{st} is composed of two different contributions: the first is due to the interactions between the adsorbate and the surface and the second is due to the interactions between the adsorbed molecules. For $0.5 < \theta < 1$, the increase of q^{st} indicates that adsorbate−adsorbate interactions rise gradually as the surface coverage increases. Conversely, the decrease of q^{st} for $\theta > 1$ is due to the multilayer formation for which the interactions between the adsorbate and the ice surface become weaker.

Figure 5 shows infrared difference spectra in the ν(OH) region for different CO coverages. As the adsorbed amount increases, three bands centered at 3696, 3563, and 3489 cm^{-1} decrease

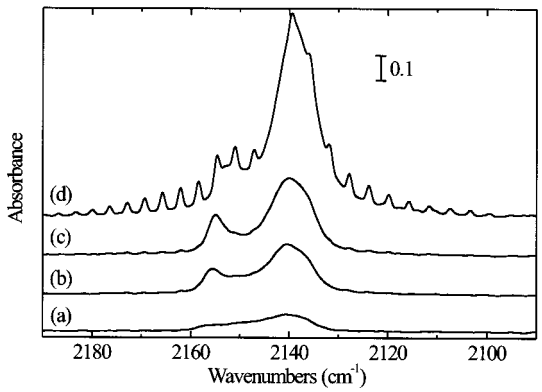

Figure 6. Infrared difference spectra (CO adsorbed on ice at $T = 56.3$ K minus bare ice) in the region of CO vibration for surface coverage θ (a) 0.21, (b) 0.73, (c) 0.92, and (d) 3.80.

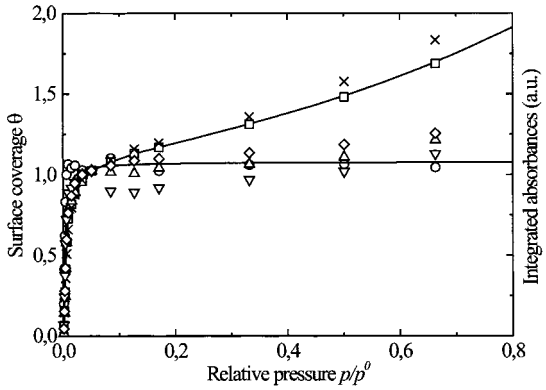

Figure 7. Volumetric (□) and infrared isotherms of ice and CO at $T = 56.3$ K for the dH (○), dO (▽), and s4 (▽) ice bands and for the 2154 (◇) and 2139 cm^{-1}(×) CO bands. The continuous lines are only guide for the eyes.

and a new band appears at 3636 cm^{-1}. These bands have already been observed by Devlin's group[11,40,41] and have been assigned to the OH vibration of the three surface modes mentioned above. The band at 3696 cm^{-1} caused by the dH mode of bare ice is red-shifted 60 cm^{-1} because of CO uptake. The two other bands are much broader and are revealed only by these difference spectra. The high-frequency (respectively low-frequency) band at 3563 cm^{-1} (respectively at 3489 cm^{-1}) has been assigned to three-coordinated molecules, dO (respectively four-coordinated molecules, s4). The expected appearance of new bands is not clearly evidenced; in fact, their shifts would be too small in comparison with the bandwidth to permit them to be distinguished. Nevertheless, these results show that CO interacts not only with dH but also with all of the other sites of amorphous ice.

In the ν(CO) region (Figure 6), the signal due to adsorbed CO is intense and appears as a doublet: a main peak centered at 2139 cm^{-1} (fwhm of 8 cm^{-1}) which is close to that of solid CO and a minor component blue-shifted to 2154 cm^{-1} (fwhm of 5 cm^{-1}). These two signals are consistent with those obtained in previous studies.[15,17−19,42,43] The main peak position shows that the mode is caused by CO slightly disturbed by the ice surface and/or probably by CO interacting with other CO molecules.

For $\theta < 1$, the 2154 cm^{-1} band accounts for 25−29% of the total integrated intensity of the CO bands, and this is in good agreement with what Schmitt et al. have already measured.[15] This signal is assigned to CO interacting with the dH of the ice surface, and the blue-shift shows that a hydrogen bond has been formed. It should be noted that an analogous but stronger effect has been observed on several zeolites:[26,27] the CO stretching modes of the complexes formed with the acidic hydroxyl groups have been observed in the region 2175−2168 cm^{-1}, whereas a second band centered at 2138 cm^{-1} has been assigned to physically adsorbed CO.

In the case of ice, the band at 2139 cm^{-1} has been up to now attributed to three possible causes. According to Sandford et al.,[14] it is due to substitutional CO molecules (CO replacing H_2O molecules). It has been also tentatively assigned to CO molecules interacting with the oxygen atoms of the pore−surface water molecules.[18,42] Finally, in paper I,[19] was suggested an assignment to CO interacting with dH in an orientation other than that for the signal at 2154 cm^{-1}.

Figure 7 shows the *volumetric* and the five *infrared* isotherms which can be plotted, three of them for the three modes of ice (dH, dO, and s4) and two of them for the two modes of CO (2139 and 2154 cm^{-1}). We have chosen here to focus on the plateau to differentiate the types of isotherms, the six of them displaying similar knee shape. The three infrared isotherms of ice are type I, characteristic of a surface phenomenon: the absorbance rises at low values of p/p^0 and then reaches a horizontal plateau when monolayer completion is achieved. This confirms that the three ice signals which have been identified are caused by surface phenomenon alone and shows that there are three possible adsorption sites for CO. Moreover, displaying the same knee shape and reaching the plateau at the same relative pressure mean that these three isotherms are related to three sites having equivalent adsorption energies. The question is now to establish the relationship between the three ice signals and the two CO signals.

The CO signal at 2154 cm^{-1} provides a type I isotherm (Figure 7). The correlation between this isotherm and that of the dH signal has already been pointed out[31] and agrees with previous assignments of CO interacting with a dangling OH bond.[18,19,42] Moreover, as mentioned above, the blue-shift of the band at 2154 cm^{-1} proves that the molecule is involved in a hydrogen bond like "O−H···CO", and this kind of hydrogen bond, for which CO acts as a proton acceptor, is possible with a dH site, but not with a dO site, nor with an s4 site. The correlation of the high-frequency band of CO and that of ice is thus well established.

The CO signal at 2139 cm^{-1} provides an isotherm analogous to the type II volumetric isotherm (Figure 7). As this type of isotherms features both surface phenomena and multilayer adsorption,[44] this clearly shows that the signal at 2139 cm^{-1} does not represent a surface phenomenon alone. This signal is thus composed of several signals arising from the interactions of CO with dO and s4 sites of the ice surface and from CO−CO interactions occurring during the multilayer formation.

III. Quantum Study

A. Method of Calculation. In paper I, the PHF method and the embedded cluster method have been used to model the ice surface and the adsorption of small molecules. The calculations have been performed using CRYSTAL92 and EMBED93 computer programs. These methods have proved to reliably reproduce the cooperative and collective properties of the hydrogen bonds responsible for solid cohesion. The electronic correlation energy has been added to that obtained by a posteriori density functional calculation using the PHF density matrix in the generalized gradient approximation (GGA) and Perdew−Wang functional (PW91).[45,46] The periodic methods use a perfect surface model, but it has been shown that this approach is transferable to the real ice surfaces obtained in our laboratory,

TABLE 1: Geometric Parameters of the Optimized P−ice for PHF and DFT-PW Methods[a]

geometric data	PHF	DFT-PW
	Cell Parameters	
a	4.40	4.44
b	7.92	7.95
	OH Bond Lengths	
dH	0.93, 0.97	0.97, 1.03
s4a	0.97, 0.97	0.99, 1.03
s4b	0.97, 0.97	0.99, 1.03
dO	0.97, 0.97	0.99, 0.99
	HOH Angles	
dH	109.2	105.5
s4a	109.2	104.2
s4b	110.8	109.4
dO	110.8	107.9
	H-Bond Lengths	
s4a, PA	1.75	1.76
s4b, PA	1.82	1.81
s4b, PD	1.75	1.58

[a] The two O−H lengths of the dH, dO, and s4 molecules are indicated in Å, and their angles H−O−H are indicated in degrees. The three H-bond lengths with s4a or s4b molecules are also displayed for the dH molecule, indicating its proton acceptor (PA) or proton donor (PD) character.

at least at a semiquantitative level of approximation.[19,47,48] For instance, this method of calculation has successfully revealed that the shift of the dH mode of ice with adsorption mainly depends on the vibrational Stark effect.[49]

However these investigations have certain drawbacks. First of all, calculations are always very time-consuming, and this prevents us from studying complex systems. Moreover, the PHF computer codes do not include the automatic energy gradient calculation: the equilibrium adsorption structures are calculated by quadratic interpolation techniques, and therefore, they are "human-dependent". A last problem lies in the choice of the atomic basis sets as it is impossible to use diffuse atomic orbitals because of the quasilinear dependency. Even though this constraint is less dramatic than for molecular systems, it limits complex calculations.

In the past decade, new methods have been developed using DFT to deal with large systems. These theories are well suited to interpret experimental data, such as those obtained for molecules on surfaces. The algorithmic implementations include the plane wave basis set associated to ultrasoft pseudopotential method and efficient iterative schemes for solving the one-electron DFT equation (referred to as DFT-PW), as for example the CASTEP program developed at Cambridge University.[50]

We chose to employ this program for ice and to use the same model as in paper I: the surface of ice was represented as a two-dimensional (2D) infinite slab whose unit cell of $Pna2_1$ symmetry, containing 24 atoms with the three sorts of surface molecules (dH, dO, and s4), was that optimized by the Turin group.[51,52] Using a fully ordered ice surface to model the real surface allows us to reduce the CPU time and has already proved to successfully reproduce the experimental results.[48,49] This is probably because it has the advantage of taking all of the chemical environments into account.

The P−ice structure was therefore reoptimized using the new method of calculation. Six *k* points were taken for the Brillouin zone sampling, with the number of plane waves per *k* point varying between 6127 and 6168. The exchange-correlation energy was evaluated by the GGA-PW91 density functional, and the cutoff energy was fixed at 300 eV. The PHF and DFT-PW cell geometric parameters are compared in Table 1. The values are very close and do not differ by more than 0.04 Å which shows that the two methods provide similar structures. However, it should be noted that the DFT-PW method leads to an increase in covalent bond length ranging from 4% for free OH to 6% for H-bonded OH, in agreement with the behavior generally observed when comparing DFT and PHF results. The most important change lies in the hydrogen bond length of the dH type molecule. The H-bond where the dH molecule acts as a proton donor (cf. Table 1) decreases to 1.58 Å, revealing a greater acidity.

TABLE 2: Adsorption Energies (kJ mol^{-1}) and Geometrical Parameters (Å) for the Two Orientations of CO above dH Calculated with PHF and DFT-PW Methods

	PHF	DFT-PW
	Adsorption Energies	
OC···HOH	10.9	11.4
CO···HOH	5.0	5.1
	Lengths	
OC···HOH	2.04	2.19
C−O	1.11	1.14

In what follows, two types of energy are used. The first is the interaction energy between the adlayer and the surface, defined by

$$\Delta E_{\text{int}} = \frac{E_{\text{ice}} + E_{\text{layer}} - E_{\text{tot}}}{N} \tag{4}$$

where N is the number of adsorbed molecules per cell, E_{ice} is the energy of the ice alone, E_{tot} is the energy of the complete system containing ice and the CO layer, and E_{layer} is the energy of the CO layer alone. The second is the dissociation energy, defined by

$$\Delta E_{\text{dis}} = \frac{E_{\text{ice}} + \sum_s E_{\text{CO}} - E_{\text{tot}}}{\text{N}} \tag{5}$$

where *s* refers to the different sites of the cell.

ΔE_{int} covers only perpendicular CO−ice interactions, whereas ΔE_{dis} covers both perpendicular CO−ice and lateral CO−CO interactions and then will be compared in the discussion to the adsorption energy deduced from experiments.

B. Adsorption of Carbon Monoxide. *1. One Molecule per Unit Cell.* In paper I, the adsorption process has been simulated with one molecule per unit cell. Two minima have been found for CO perpendicular to the surface and above the dH molecule, interacting with C or with O next to the surface, with the first position being the most stable. The DFT-PW calculation confirms these results remarkably well (Table 2 and Figure 8a). The discrepancy is less than 0.5 kJ mol^{-1} for the energy and 0.15 Å for the distance between the surface and the admolecule, whereas bond lengths are slightly larger than those for PHF. The good agreement between the two methods may be surprising, but it is explained by the following reasons: (i) the same equilibrium configuration is found by the two different ways and (ii) the exchange-correlation energy is calculated with the same density functional.

The adsorption of CO upon the dH molecule, with O next to the surface, leads to an interaction energy of 5.1 kJ mol^{-1}, which is 6.3 kJ mol^{-1} less stable than the other position (11.4 kJ mol^{-1}). This type of adsorption geometry (i.e., above the dH bond) will be called dH site in what follows and only the most stable CO position will be considered. Nevertheless, these results are valid only if lateral interactions between admolecules belonging to neighboring unit cells are negligible, which is

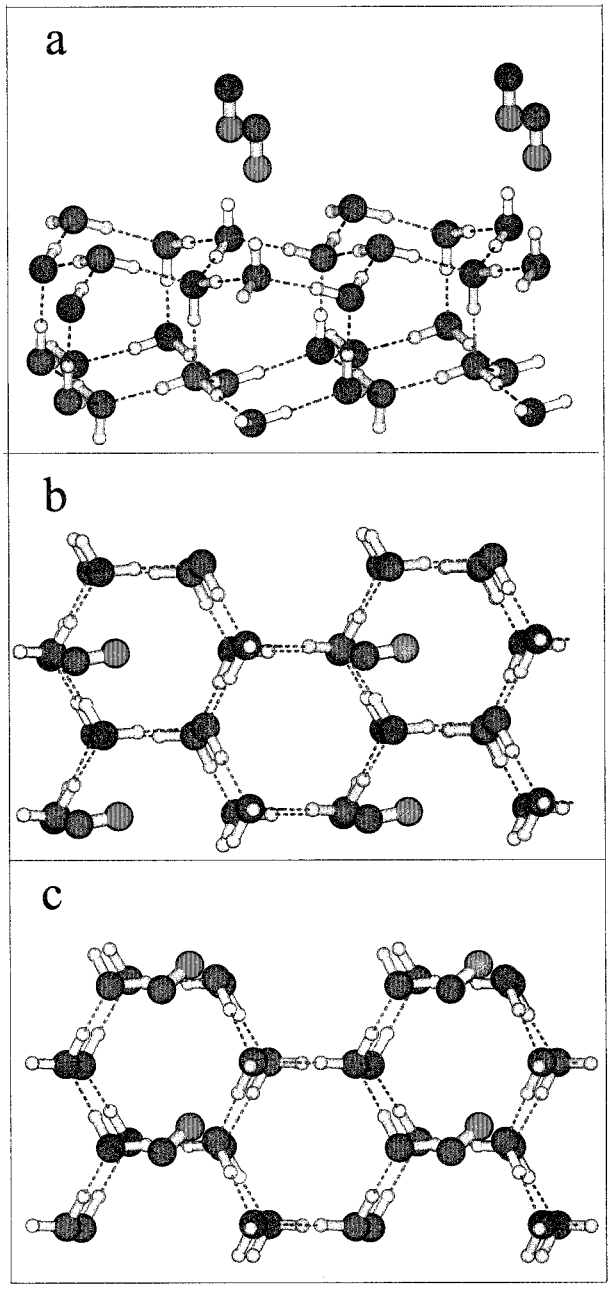

Figure 8. Adsorption of one CO per cell. Views of the three calculated site structures: (a) dH−CO; (b) top view of s4−CO; and (c) top view of dO−CO.

expected from experimental considerations.[19] This approximation can be quantified here by performing the same calculation with only one CO per doubled or quadrupled cell. In both cases, we have found the geometry of the most stable conformation unchanged and interaction energy ΔE_{int} at 12.1 kJ mol^{-1}, only 0.7 kJ mol^{-1} more than when there is one CO per cell. The double (respectively quadruple) cell contains 48 (respectively 96) atoms, and thus, this type of calculation is very CPU time consuming. Because the modifications induced by introducing super cells are weak, we have not taken the interaction between similar molecules in different cells into account here. In fact, the repulsion energy is 1.4 kJ mol^{-1} for nearest neighbor molecules (4.44 Å distant), whereas it is 0.9 kJ mol^{-1} for neighboring molecules in perpendicular direction (7.95 Å distant).

A second stable position is found where the admolecule is roughly parallel to the surface (Figure 8b), above an s4 water molecule (s4a site in Figure 1). Both O and C atoms of CO are at roughly equal distance from the s4 O atom (respectively 3.54 and 3.42 Å) and the CO bond length is, as for the first position, 1.14 Å. The distances to the nearest hydrogen atoms range from 3.21 to 3.34 Å, thus excluding the formation of hydrogen bonds. The stability of the system is entirely caused by electrostatic interactions which lead to an interaction energy ΔE_{int} of 9.6 kJ mol^{-1}.

TABLE 3: Interaction Energy ΔE_{int} and Dissociation Energy ΔE_{dis} in kJ mol^{-1} for Various Numbers of CO Molecules Per Cell

CO per cell	ΔE_{int}	ΔE_{dis}
1	11.4	11.4
2	12.2	13.3
3	9.8	9.9
4	7.4	8.1

A third optimized structure is found for CO tilted with respect to the surface plane at equal distance from the dO and from the s4b molecules (Figure 8c). The C (respectively O) atom is 3.51 Å (respectively 4.20 Å) from the s4b O atom and 3.76 Å (respectively 3.79 Å) from the dO O atom. As for the preceding position, the interaction energy ΔE_{int} (10.6 kJ mol^{-1}) is of electrostatic origin alone. For the sake of simplicity, this adsorption site will be called the dO site and CO interacting with ice in the three stable geometries described above will be referred to as respectively dH−CO, s4−CO, and dO−CO.

Only dH−CO has been found stable in paper I, with the optimization procedure being performed at the PHF level with the dispersion contribution then simply added to the minimum energy. In the DFT-PW model, the dispersion contribution is mainly provided by the electronic correlation energy and is therefore always taken into account throughout the calculations presented here. This is probably why two additional stable structures have been found with this method. The discrepancy induced by the two methods is also due to the basis set superposition error (BSSE), and it is well-known that, in the case of very weak interaction, the BSSE correction can be larger than the intermolecular energy. In fact, especially when the admolecule is flat above the crystal surface, the PHF method tends to overestimate the counterpoise correction. This point has been more thoroughly analyzed in the case of adsorption of acetone and formaldehyde on ice.[53]

Another site has been investigated above the canal of the ice surface cell. As in paper I, no stable configuration has been found, the molecule always moving toward one of the sites already described.

Summing up on this point, we have found three configurations for the adsorption of a single CO molecule per unit cell, whose energies are similar. Thus, the three structures may be considered with roughly the same probability, at least at the present level of approximation. The aim of this work was to investigate how the admolecules cover the ice surface and to propose a quantum model for the structure of the monolayer. The dH−CO configuration will be arbitrarily chosen for describing the case of one CO per cell (the values of ΔE_{int} and ΔE_{dis} in this case are reported in Table 3).

2. Higher Surface Coverages. We have tried to find the configuration for higher coverage by adding a second molecule within the cell. We will compare energies found for two molecules per cell with those obtained for one molecule per cell in the case of dH-CO. It is well-known that two interacting quadrupolar molecules preferentially adopt an L-type configuration; this thus eliminates the possibility of combining dO- and s4-CO which are nearly parallel. One of the admolecule is

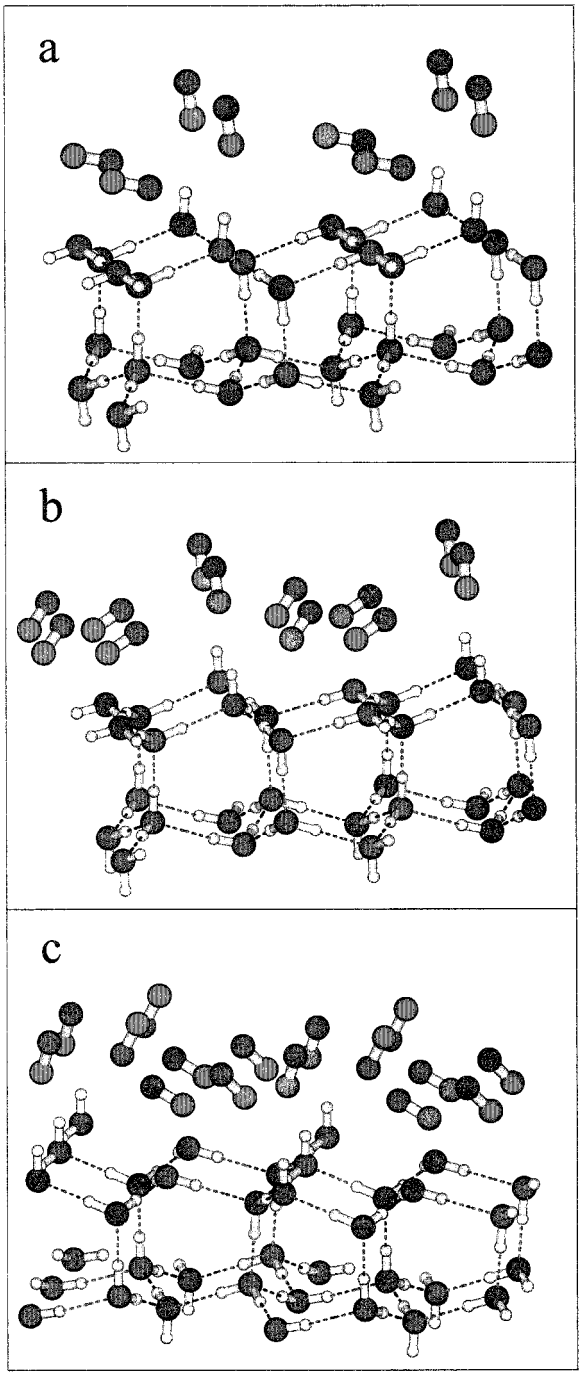

Figure 9. Adsorption of several CO per cell. View of the calculated structures: (a) two CO per cell in the dH−s4 configuration; (b) three CO per unit cell; and (c) four CO per unit cell.

therefore a dH-CO, whereas the other is a dO- or an s4-CO. Moreover, s4 molecules being nearer dH than dO, the dH-s4 interaction will be more efficient than dH-dO. The geometrical structure issued from the optimization process is displayed in Figure 9a. CO bond lengths are still 1.14 Å, and the two admolecules are 3 Å distant. When comparing with one molecule per cell, the dH-CO is no more exactly perpendicular to the surface and the s4-CO is closer to the surface, with these modifications being propitious to both CO−CO and CO−ice interactions. ΔE_{int} is 12.2 kJ mol^{-1}, 0.8 kJ mol^{-1} more stable than when there is one molecule per cell, whereas ΔE_{dis} is 13.3 kJ mol^{-1} (Table 3). The difference between these two values (1.1 kJ mol^{-1}) indicates that lateral interaction now contributes to the cohesive energy of the adlayer.

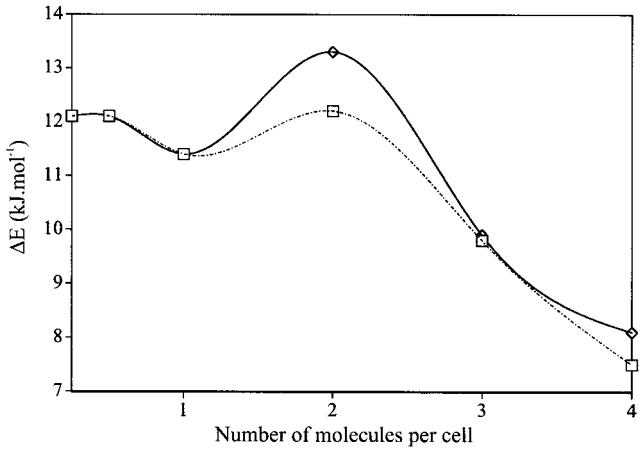

Figure 10. Calculated interaction energy ΔE_{int} (□) and dissociation energy ΔE_{dis}(◇) as functions of the number of CO per cell. The first two points are the values obtained in the cases of double and quadrupole cells.

Adding a third molecule leads to the geometry shown in Figure 9b. The extra CO adsorbs between a dO and an s4 molecule in a way analogous to the so-called dO-CO described in the former paragraph. The two molecules flat on the surface are antiparallel in a distorted L position with respect to dH-CO. Both ΔE_{int} and ΔE_{dis} decrease (Table 3), meaning that this new electronic distribution is less propitious to the ice−adlayer interaction and also that intralayer repulsions are emerging.

A fourth molecule can be adsorbed above the ice canal (Figure 9c), which is not a stable site when there is only one CO per cell. By adding a fourth molecule, both ΔE_{int} and ΔE_{dis} decrease but the former more than the latter (Table 3), showing that the CO−CO intralayer interaction become larger. No more room is available on the ice surface, and the completion of the ideal surface is thus reached with four molecules per cell.

C. Discussion. It should be noted that all of the interaction energies involved in the processes described above are weak, near the limit of the accuracy of calculations, and therefore, the discussion can be developed only at a semiquantitative level. We have tried to increase the energy cutoff as well as the *k* point sampling, and the general trend remains unchanged. For example, using a finer integration grid and a larger *k*-point distribution to optimize the ice crystal unit cell leads to a change of about 0.02 Å in the bond lengths.

Figure 10 represents ΔE_{int} and ΔE_{dis} as a function of the number of COs per cell and summarizes all of the physical aspects encountered during this study. Choosing the starting structure (up to one molecule per cell) as dH−CO can seem somehow arbitrary because dO−CO and s4−CO have similar adsorption energies. Conversely, in the case of two COs per cell, the gain in energy is larger for the dH−s4 L-type structure (2.5 kJ mol^{-1}) than for the dH−dO (respectively dO−s4) structure (−0.1 kJ mol^{-1}, respectively −1.8 kJ.mol^{-1}). Therefore, the more numerous dH−s4, the more stable the layer, and another choice would lead to a similar maximum of energy. Figure 10 shows that (i), up to one molecule per cell, the carbon monoxide can be considered as isolated on the surface and can adopt any of the three optimized configurations; (ii) in the case of two molecules per cell, the structure is more stable, and this is mainly caused by the lateral CO−CO stabilizing interaction; (iii) for three molecules per cell, both the vertical and the lateral interactions decrease, revealing lateral repulsive intermolecular contributions; and (iv) when the unit cell contains four molecules, the adlayer as a whole is less bonded to the ice

surface but the intermolecular interaction begins increasing again, with the last adsorbed molecule being bonded to a great extend through this contribution.

At higher surface coverage, throughout the solid formation, a fifth molecule will adsorb on an upper layer and ΔE_{dis} will rise toward the cohesive energy of solid carbon monoxide, calculated at 10.1 kJ mol^{-1} by the same method.

IV. General Discussion

Infrared data have clearly evidenced three bands decreasing throughout adsorption, with their corresponding infrared isotherms being type I. This has confirmed their previous attribution as surface signals.[11] It should be noted that this evolution is reversible and all of the amount of CO can be desorbed, showing unambiguously pure physisorption and absence of diffusion into the bulk. Calculations have evidenced also three stable adsorption sites for CO isolated on the ice surface whose geometries agree rather well with the experimental attribution to adsorption on dH, s4, or dO surface molecule. In the case of the dH− or s4−site, calculations have shown that CO is roughly above the dH or s4 water molecule, whereas in the case of dO, the actual geometry is halfway between that of adsorption on a dO and on an s4 molecule. The shape of the knees is identical for the three infrared isotherms, showing both that CO interacts with the three sites simultaneously and that their adsorption energy is similar. The value of adsorption energy, as deduced from a BET fit of the volumetric isotherm, is 11.4 kJ mol^{-1} and represents a mean value for the different sites. These results are in agreement with the theoretical results which predict close values for the three sites at 11.4, 10.6, and 9.6 kJ mol^{-1}, with the precise values of the energy difference being obviously meaningless taking the accuracy of this type of calculations into account.

The questions arising from these observations are now, is the simultaneous evolution of the infrared signals caused by a simultaneous adsorption on the three sites, showing thus a nonselective adsorption, or is it caused by a delocalized interaction of CO with the whole surface, whatever the exact adsorption site is? There are nevertheless experimental indications showing independent behavior of the three infrared signals. First, the dH mode position and bandwidth clearly prove that it is very weakly coupled with the other surface modes and that, in like manner, the modification induced by the interaction with CO is localized. Second, we have also performed successive adsorptions with different adsorbates preceding CO,[32] and we have measured the decrease of integrated absorbance of the three bands throughout the CO adsorption. The ratios between these intensities strongly depend on the preadsorbate and are also different from those obtained for pure CO adsorption. The evolution of the three sites is thus independent, and this validates the model of adsorption on specific sites. No site selectivity is nevertheless evidenced due to the similarity of the adsorption energies.

Only two infrared bands have been observed for CO, whereas there are three for ice O−H stretchings. We have identified a type I isotherm for the high-frequency band at 2154 cm^{-1} and a type II for the low-frequency band at 2139 cm^{-1}. The latter behavior points out the multiplicity of the band at 2139 cm^{-1}, originating from both surface and multilayer. The band at 2154 cm^{-1} being due to CO interacting with dH, the surface contribution of the band at 2139 cm^{-1} is therefore due to the two other interactions with dO and s4. The position of this band is consistent with the expected weak interaction with the electron donor site (dO) or with the saturated site (s4). It is also consistent with the hypothesis of multilayer contribution, which is expected to be close to solid CO.

We have tried to calculate the CO vibrational frequencies for the three adsorption sites optimized by CASTEP in the case of three CO per cell, using the Gaussian 98[54] program with the same PW91 density functional but replacing the plane wave basis set by the standard 6-31G(d,p) Gaussian basis set. The influence of the ice is only taken into account through the CO vibrator bond length. The approximations are therefore very coarse, and the quantitative results have to be taken with a great care. We have obtained dH−CO vibration at 2194 cm^{-1} (exp. 2154 cm^{-1}), dO−CO at 2168 cm^{-1} (exp. 2139 cm^{-1}), and s4−CO at 2159 cm^{-1} (exp. 2139 cm^{-1}). A semiquantitative agreement is thus found, with the two theoretical values of dO− and s4−CO being only 9 cm^{-1} distant, whereas the dH−CO value is at a much higher frequency. Moreover, the three calculated infrared intensities are respectively 71, 108, and 64 km mol^{-1}. For a surface coverage less than a monolayer, as checked with the adsorption isotherm, the experimental band at 2154 cm^{-1} nearly accounts for a third of the total integrated intensity of CO bands. This is consistent with calculated infrared intensities if we compare that of dH−CO (71 km mol^{-1}) with the sum of those of s4−CO and dO−CO (172 km mol^{-1}).

We will now discuss the comparison between Figures 4 and 10 displaying adsorption energy as a function of the surface coverage, as deduced from experiments and calculations, respectively. Both curves have similar shape, showing a maximum of 11.4 and 13.3 kJ mol^{-1}, respectively, in a satisfactory agreement, taking the accuracy of both experiments and calculations into account. It is interesting to analyze how calculations enlighten the origin of the evolution in energy throughout the adsorption process. For low coverage, the energy increases as the surface coverage increases. This is due to the appearance of CO−CO lateral interactions and also to an increase of CO−surface interactions as indicated by the values of ΔE_{int} (Table 3). For high coverage, the energy decreases as the surface coverage increases. CO−ice interactions decrease, whereas CO−CO interactions dominate and become repulsive. Finally, calculations show that the monolayer is stabilized not only by the CO−ice interactions but also, and even mainly, by the lateral interactions. This explains why a fourth molecule can adsorb above the canal, whereas this position is not stable if there is no other preadsorbed molecule. The calculated monolayer structure shows a high compacity with four molecules per cell due to the specific L−type arrangement of quadrupolar CO in agreement with the higher monolayer capacity measured for CO than for spherical molecules.[32] The mean nearest neighbor distance between CO molecules is calculated at 3.74 Å for the full monolayer, whereas it is 3.99 Å for solid CO. This shows that the CO layer network is forced by the ice network despite the weakness of the interactions, with vertical relaxation of CO positions allowing the final compacity to be achieved.

The maximum of adsorption energy is found for $\theta = 0.8$ in the case of experiments and for two molecules per cell (i.e., $\theta = 0.5$) in the case of calculations. This difference probably originates from the arbitrary choice of surface filling in calculations. We have indeed chosen only dH−CO for the case of one molecule per cell, whereas dH−CO, s4−CO, and dO−CO have similar energies and should have roughly the same probability. The maximum of adsorption energy is mainly due to the stabilization induced by the dH−s4 L−type arrangement. If we assume a statistical filling for one molecule per cell (i.e., $^1/_3$dH, $^1/_3$dO, and $^1/_3$s4), the stabilization will occur through the

maximum number of occupied dH−s4 configurations, i.e., for more than two molecules per cell, as observed for experiments. Finally, we should also keep in mind that the actual surface of amorphous ice probably contains a great amount of defaults, providing another reason for the discrepancy between experiments and calculations.

V. Conclusion

The aim of this paper was to take advantage of using new experimental and theoretical methods to revisit CO adsorption on amorphous ice. Calculations based on DFT using plane wave basis set and ultrasoft pseudopotentials, readily taking dispersion into account, have allowed to determine three adsorption sites, whose structures agree with information deduced from ice and CO vibrational spectroscopy. Measuring infrared isotherms have given results confirming previous infrared assignments and allowing the origin of the two CO vibrational bands to be analyzed in more detail. The multilayer formation occurring during adsorption is clearly shown to contribute to the low-frequency band. A theoretical estimation of infrared intensities have shown that modeling an amorphous ice surface by the perfect surface described by Pisani et al.[51] is useful for describing the actual adsorption sites experimentally observed. A simultaneous growth of CO on the three sites has been evidenced by experiments for the early stages of adsorption, consistently with the similarity of the three calculated adsorption energies, revealing the weakness of the H bond between dH and CO and the absence site selectivity. The high compacity of the monolayer structure induced by the ice network has been explained by specific interactions due to the quadrupolar moment of CO.

We believe that the theoretical method used here has succeeded in pointing out the physical mechanisms involved in the adsorption and in providing information on the way of the monolayer filling. These calculations have proved to be a fruitful tool for deepening understanding of experiments and have the advantage of being easily transferable to other large systems. For instance, CO adsorption will be compared with various other gas adsorption in a forthcoming paper.

Acknowledgment. We friendly acknowledge Prof. J. Pourcin for giving the first impetus to this work. We also wish to have a special thought for the memory of P. Verlaque who has managed in doing the first experiments.

References and Notes

(1) Fukazawa, H.; Sugiyama, K.; Mae, S. *Geophys. Res. Lett.* **1998**, *25*, 2845.

(2) Fukazawa, H.; Mae, S.; Ikeda, S.; Watanabe, O. *Chem. Phys. Lett.* **1998**, *294*, 554.

(3) Taylor, R. S. M.; Gilligan, J. J.; Moody, D. J.; Castleman, A. W. *J. Phys. Chem. A* **1999**, *103*, 4196.

(4) Livingston, F. E.; George, S. M. *J. Phys. Chem. B* **1999**, *103*, 4366.

(5) Curry, J. A.; Radke, L. F. *Atmos. Environ.* **1993**, *27A*, 2873.

(6) Takahashi, J.; Nagaoka, M.; Masuda, K. *Int. J. Quantum Chem.* **1998**, *70*, 379.

(7) Brooke, T. Y.; Tokunaga, A. T.; Weaver, H. A.; Crovisier, J.; Bockelee-Morvan, D.; Crisp, D. *Nature* **1996**, *383*, 606.

(8) Hudson, R. L.; Moor, M. H. *Icarus* **1997**, *126*, 233.

(9) Moore, M. H.; Hudson, R. L. *Icarus* **1998**, *135*, 518.

(10) van Dishoeck, E. F. *Faraday Discuss.* **1998**, *109*, 31.

(11) Devlin, J. P.; Buch, V. *J. Phys. Chem.* **1995**, *99*, 16534.

(12) Rowland, B.; Fisher, M.; Devlin, J. P. *J. Chem. Phys.* **1991**, *94*, 812.

(13) Buch, V.; Devlin, J. *J. Chem. Phys.* **1991**, *94*, 4091.

(14) Sandford, S. A.; Allamandola, L. J.; Tielens, A. M.; Valero, G. J. *Astrophys. J.* **1988**, *329*, 498.

(15) Schmitt, B.; Greenberg, J. M.; Grim, R. J. A. *Astrophys. J.* **1989**, *340*, L33.

(16) Devlin, J. P. *J. Phys. Chem.* **1992**, *96*, 6185.

(17) Givan, A.; Loewenschuss, A.; Nielsen, C. J. *J. Chem. Soc., Faraday Trans.* **1996**, *92*, 4927.

(18) Palumbo, M. E. *J. Phys. Chem. A* **1997**, *101*, 4298.

(19) Allouche, A.; Verlaque, P.; Pourcin, J. *J. Phys. Chem. B* **1998**, *102*, 89.

(20) Haq, S.; Love, J. G.; King, D. A. *Surf. Sci.* **1992**, *275*, 170.

(21) Chang, H.-C.; Richardson, H. H.; Ewing, G. E. *J. Chem. Phys.* **1988**, *89*, 7561.

(22) Noda, C.; Richardson, H. H.; Ewing, G. E. *J. Chem. Phys.* **1990**, *92*, 2099.

(23) Heidberg, J.; Kampshoff, E.; Suhren, M. *J. Chem. Phys.* **1991**, *95*, 9408.

(24) Zecchina, A.; Coluccia, S.; Spoto, G.; Scarano, D.; Marchese, L. *J. Chem. Soc., Faraday. Trans.* **1990**, *86*, 703.

(25) Marchese, L.; Coluccia, S.; Martra, G.; Zecchina, A. *Surf. Sci.* **1992**, *269/270*, 135.

(26) Kustov, L. M.; Kaznsky, V. B.; Beran, S.; Kubelkova, L.; Jiru, P. *J. Phys. Chem.* **1987**, *91*, 5247.

(27) Zecchina, A.; Bordiga, S.; Spoto, G.; Scarano, D.; Petrini, G.; Leofanti, G.; Padovan, M.; Arean, C. O. *J. Chem. Soc., Faraday Trans.* **1992**, *88*, 2959.

(28) Echoufi, N.; Gélin, P. *J. Chem. Soc., Faraday Trans.* **1992**, *88*, 1067.

(29) Lane, G. S.; Miller, J. T.; Modica, F. S.; Barr, M. K. *J. Catal.* **1993**, *141*, 465.

(30) Neyman, K. M.; Strodel, P.; Ruzankin, S. P.; Schlensog, N.; Knözinger, H.; Rösch, N. *Catal. Lett.* **1995**, *31*, 273.

(31) Manca, C.; Roubin, P.; Martin, C. *Chem. Phys. Lett.* **2000**, *330*, 21.

(32) Martin, C.; Manca, C.; Roubin, P. *Surf. Sci.*, accepted.

(33) Sadlej, J.; Rowland, B.; Devlin, J. P.; Buch, V. *J. Chem. Phys.* **1995**, *102*, 4804.

(34) Rozenberg, M.; Loewenschuss, A.; Marcus, Y. *Langmuir* **1999**, *15*, 5454.

(35) Devlin, J. P.; Sadlej, J.; Buch, V. *J. Phys. Chem. A* **2001**, *105*, 974.

(36) Brunauer, S.; Emmett, P.; Teller, E. *J. Am. Chem. Soc.* **1938**, *60*, 309.

(37) Rouquerol, F.; Rouquerol, J.; Sing, K. *Adsorption by powders and porous solids*; Academic Press: London, 1999.

(38) Nair, N.; Adamson, A. *J. Phys. Chem.* **1970**, *74*, 2229.

(39) Clayton, J.; Giauque, W. *J. Am. Chem. Soc.* **1932**, *54*, 2610.

(40) Delzeit, L.; Devlin, M. S.; Rowland, B.; Devlin, J. P.; Buch, V. *J. Phys. Chem.* **1996**, *100*, 10076.

(41) Devlin, J. P.; Buch, V. *J. Phys. Chem. B* **1997**, *101*, 6095.

(42) Devlin, J. P. In *Physics and Chemistry of Ice*; Maeno, N., Hondoh, T., Eds.; Hokkaido University Press: Sapporo, Japan, 1992; p 183.

(43) Givan, A.; Loewenschuss, A.; Nielsen, C. J. *Vib. Spectrosc.* **1998**, *16*, 85.

(44) Sing, K. S. W.; Evrett, D. H.; Haul, R. A. W.; Moscou, L.; Pierotti, R. A.; Rouquérol, J.; Siemieniewska, T. *Pure Appl. Chem.* **1985**, *57*, 603.

(45) Perdew, J.; Wang, Y. *Phys. Rev. B* **1986**, *33*, 8800.

(46) Perdew, J. P. In *Electronic structure of solids*; Ziesche, P., Eschrig, H., Eds.; Akademic Verlag: Berlin, Germany, 1991.

(47) Allouche, A. *J. Phys. Chem. A* **1999**, *103*, 9150.

(48) Borget, F.; Chiavassa, T.; Allouche, A.; Aycard, J. P. *J. Phys. Chem. B* **2001**, *105*, 449.

(49) Manca, C.; Allouche, A. *J. Chem. Phys.* **2001**, *114*, 4226.

(50) Milman, V.; Winkler, B.; White, J.; Pickard, C.; Payne, M.; Akhmatskaya, E.; Nobes, R. *Int. J. Quantum Chem.* **2000**, *77*, 895.

(51) Pisani, C.; Casassa, S.; Ugliengo, P. *Chem. Phys. Lett.* **1996**, *253*, 201.

(52) Casassa, S.; Ugliengo, P.; Pisani, C. *J. Chem. Phys.* **1997**, *106*, 8030.

(53) Marinelli, F.; Allouche, A. *Chem. Phys.* **2001**, *272*, 137.

(54) Frisch, M. J.; Trucks, G. W.; Schlegel, H. B.; Scuseria, G. E.; Robb, M. A.; Cheeseman, J. R.; Zakrzewski, V. G.; Montgomery, J. A., Jr.; Stratmann, R. E.; Burant, J. C.; Dapprich, S.; Millam, J. M.; Daniels, A. D.; Kudin, K. N.; Strain, M. C.; Farkas, O.; Tomasi, J.; Barone, V.; Cossi, M.; Cammi, R.; Mennucci, B.; Pomelli, C.; Adamo, C.; Clifford, S.; Ochterski, J.; Petersson, G. A.; Ayala, P. Y.; Cui, Q.; Morokuma, K.; Malick, D. K.; Rabuck, A. D.; Raghavachari, K.; Foresman, J. B.; Cioslowski, J.; Ortiz, J. V.; Stefanov, B. B.; Liu, G.; Liashenko, A.; Piskorz, P.; Komaromi, I.; Gomperts, R.; Martin, R. L.; Fox, D. J.; Keith, T.; Al-Laham, M. A.; Peng, C. Y.; Nanayakkara, A.; Gonzalez, C.; Challacombe, M.; Gill, P. M. W.; Johnson, B. G.; Chen, W.; Wong, M. W.; Andres, J. L.; Head-Gordon, M.; Replogle, E. S.; Pople, J. A. *Gaussian 98*, revision A.7; Gaussian, Inc.: Pittsburgh, PA, 1998.